X-ray computerized tomography analysis and density estimation using a sediment core from the Challenger Mound area in the Porcupine Seabight, off Western Ireland

Akiko Tanaka, Tsukasa Nakano, and Ken Ikehara

Geological Survey of Japan, AIST, Tsukuba Central 7, 1-1-1 Higashi, Tsukuba 305-8567, Japan

X-ray computerized tomography (CT) analysis was used to image a half-round core sample of 50 cm long recovered from near Challenger Mound in the Porcupine Seabight, off western Ireland during the Integrated Ocean Drilling Program Expedition 307. This allowed three-dimensional examination of complex shapes of pebbles and ice-rafted debris in sedimentary sequences. X-ray CT analysis was also used for the determination of physical properties; a comparison between bulk density by the mass-volume method and estimated density based on linear attenuation coefficients of X-ray CT images provides insight into a spatially detailed and precise map of density variation in samples through the distribution of CT numbers.
Key words: X-ray CT, bulk density, sediment core, Integrated Ocean Drilling Program (IODP), Expedition 307.

1. Introduction

X-ray computerized tomography (CT) is a non-destructive technique that allows three-dimensional visualization of internal structures of samples, determined mainly by variations in their density and atomic composition. Since X-ray CT was developed as a medical imaging technique in the early 1970s (Hounsfield, 1973), it is increasingly used and has proven useful in the field of earth sciences (e.g., Mees *et al.*, 2003). For example, it has been used to present quantitative aperture data for three-dimensional intercon-nected fracture networks (Pyrak-Nolte *et al.*, 1997), to image the internal structure of fragile sea-floor hydrothermal vent samples (Tivey and Singh, 1997), and to provide information on the physical properties of sediment cores (e.g., Orsi *et al.*, 1994). Through the Ocean Drilling Program (ODP) and the Integrated Ocean Drilling Program (IODP), X-ray CT system has gained acceptance as a routine core analysis tool, and some attempts have been made to evaluate X-ray CT imaging for observation and description of core samples (e.g., Ashi, 1997; Iturrino *et al.*, 2004; Tanaka and Nakano, 2009). However, many studies were treated X-ray CT images only as a non-invasive imaging tool.

In this paper, three-dimensional imaging analysis of sediment core from the IODP Expedition 307 was performed by a medical X-ray CT system, and was compared and contrasted with line-scan digital core images and X-ray radiographs to highlight some characteristics to be considered when using these data. Also, the possibility and limitation of density estimates based on X-ray attenuation is considered.

2. Sampling and Analytical Methods
2.1 Study area and core sample

Challenger Mound, a putative carbonate mound structure covered with dead deepwater coral rubble and located on the eastern slope of Porcupine Seabight on the southwest Irish continental margin (Fig. 1), was the target of scientific drilling aboard the *JOIDES Resolution* during IODP Expedition 307 in May 2005 (Ferdelman *et al.*, 2006). The aim of this expedition was to understand the origin and evolution of the cold-water coral banks in Porcupine Seabight, one of the most intensively studied provinces (e.g., Shannon *et al.*, 2001). Eleven holes at three sites with maximum depth of 245 m have been drilled on and near Challenger mound, and core sections penetrating a thick coral reef body were recovered. Drilling revealed that the mound itself consisted of repeated sequences of unstratified Pleistocene coral (*Lopheria pertusa*) floatstone-rudstone with fine-grained matrix of clay, bioclasts, and calcareous nannofossils on a sharp erosional boundary (Williams *et al.*, 2006; Kano *et al.*, 2007).

Hole U1318A (51°26.16′N, 11°33.0′W; 423 m water depth), which is located upslope from the Belgica mound province including Challenger Mound, was drilled continuously to 142.2 mbsf (meters below sea floor) to constrain the stratigraphic framework of the slope and to capture the regional environment system, and 15 cores were taken with a recovery of 90.2%. A recovered core is divided into 1.5 m sections that are numbered serially from the top. These whole-core sections were scanned with the multisensor track (MST), included Gamma ray attenuation (GRA) bulk density measurements on board in May 2005. Core U1318A-5H-Section 4 (1.5 m long) was split into halves, referred to as "archive-half" and "working-half", on board in May 2005. Whole-core photographs of the "archive-halves"
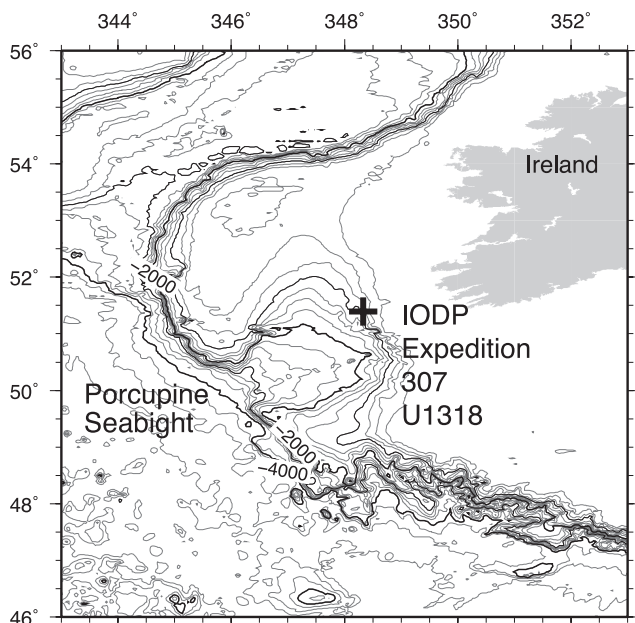
Fig. 1. Study site in Porcupine Seabight on the southwest Irish continental margin (250-m contour intervals). The cross indicates the drilling location during Integrated Ocean Drilling Program (IODP) Expedition 307 in May 2005.
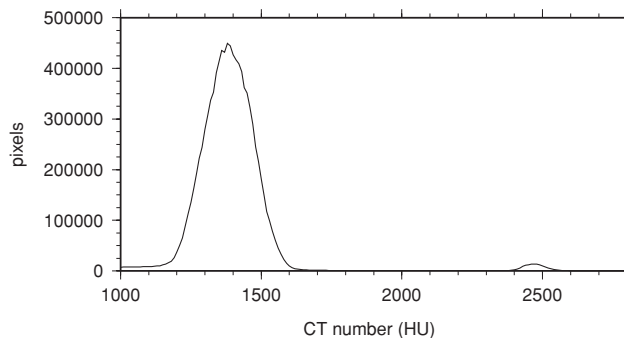

Fig. 2. Histogram of CT numbers for the half-round core sample from Section 307-U1318A-5H4, 22–72 cm. Peaks around 1380 and 2460 correspond to the host sediments and pebbles, respectively.

tained.

A medical X-ray CT scanner (Hitachi CT-W2000) of the Geological Survey of Japan, AIST, was used to acquire the CT images. A medical X-ray CT system such as used in this study was originally designed for use on human subjects to image soft tissue and bone. Cores used in this study consist mainly of sediments with densities of ~ 2 g/cm^3, which is consistent with that of human bone. It might be reasonable to use medical X-ray for internal structures of wet sediments.

All samples were scanned with X-ray peak energy of 120 kV with 150-mA current, with an in-plane resolution of 0.313×0.313 mm^2/pixel and the slice thickness of 1 mm. Slice acquisition times were 4 seconds per scan and a 160-mm field of reconstruction was captured in a 512 pixel $\times$ 512 pixel image. 545 contiguous two-dimensional 16-bit CT images at intervals of 1 mm sequentially from core top to bottom perpendicular to the longitudinal axis of the core were acquired in October 2005. These data were used to reconstruct the three-dimensional images. After image reconstruction, relative values of linear attenuation coefficient are stored for each voxel.

The intensity of the transmitted X-ray beam is usually expressed as CT number, Hounsfield unit (HU). The HU scale is a linear transformation of the original linear attenuation coefficient measurement into one where water is assigned a value of zero and air is assigned a value of -1000. When μ_{w} and μ are the linear attenuation coefficients of water and a substance of interest, the CT number is defined as HU $= 1000(\mu - \mu_{\mathrm{w}})/\mu_{\mathrm{w}}$. Thus, a change of one CT number corresponds to 0.1% of the attenuation coefficient difference between water and air. The density is the predominant factor determining X-ray attenuation at the energies of 120 kV used in this study, which is used for most medical scanners (McCullough, 1975). Therefore, each CT number represents a 0.1% changes, or approximately 0.001 g/cm^3, change in density with respect to calibration density scale.

Figure 2 shows a histogram of CT number with bin width of 10 by using 50-cm long core sample. The bin size of 10 was chosen using the histogram bin size optimization method by Shimazaki and Shinomoto (2007). Figure 2 has a single peak with a very shallow valley in the middle at around 1380. It suggests that host lithified sediments of this sample were nearly uniform in density, however
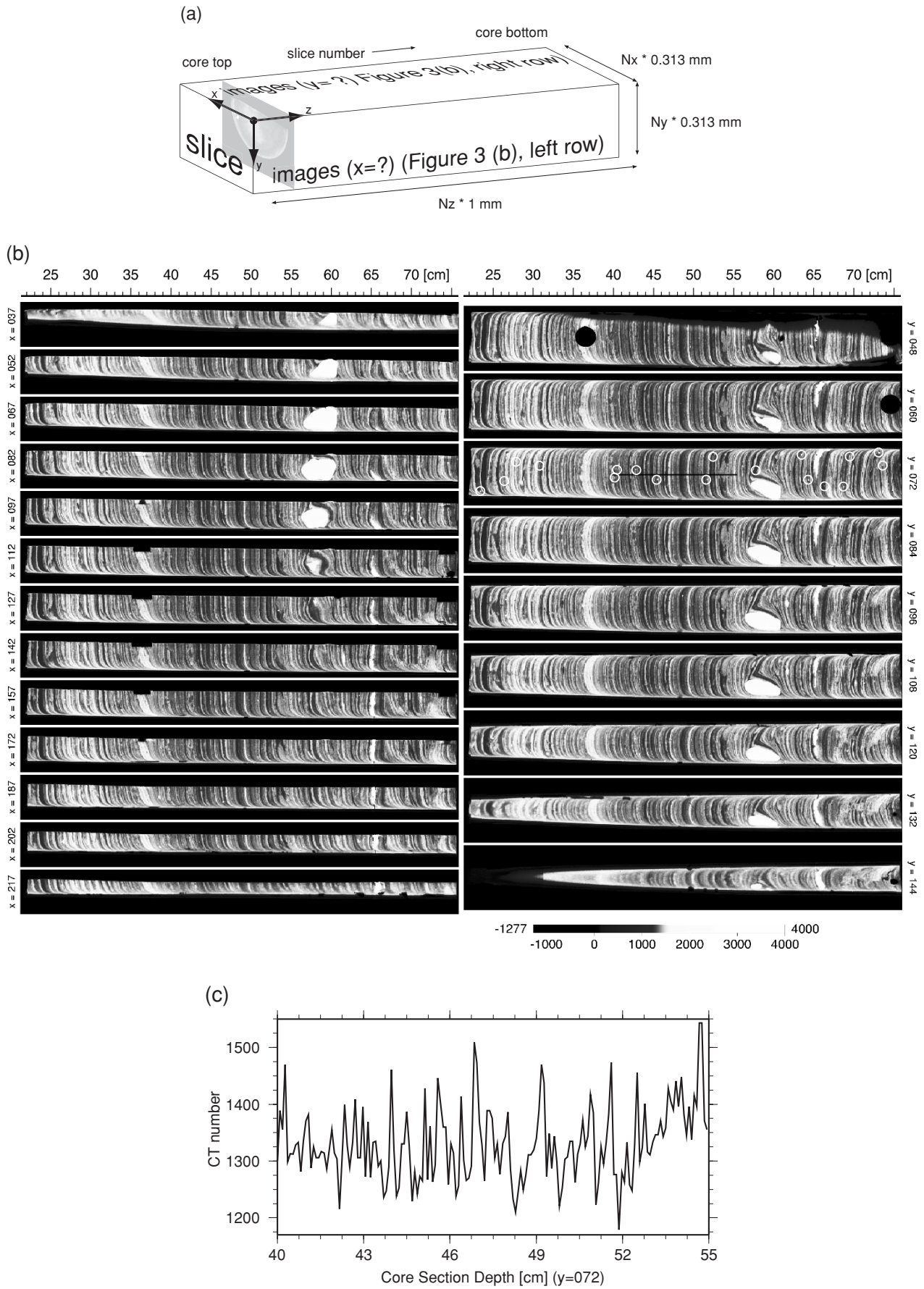
were taken on film during core description in May 2005, and subsequently line-scan digital images from the film at 3000 dpi were captured with the Digital Imaging System (http://iodp.tamu.edu/database/coreimages.html). These cores and scientific data collected by shipboard scientists were archived on the ODP/TAMU servers (ODP Information Technology and Data Services, 2007).

Half-round core sample from U1318A-5H-Section 4 was cut into 50-cm long section at the Bremen Core Repository in October 2005. This used half-round core of a diameter of 66 mm was covered with plastic shrink-wrap to avoid dry out. The allocated section 307-U1318A-5H-4, 22–72 cm (42.92–43.43 mbsf) from the upper Pleistocene clay layer, was used to know the stratigraphic sequences. This section comprises dark grayish brown to very dark gray silty clays with carbonate contents of about 15 wt% (Ferdelman *et al.*, 2006). Dropstones are much less frequent and lamination occurs on a centimeter to millimeter scale. Titschack *et al.* (2009) showed that the average sedimentation rate of this section is about 7.1 cm/ka. Assuming a constant sedimentation rate, this core sample records at intervals of about seven thousands years.

2.2 X-Ray computerized tomography measurements

X-ray CT is a radiological imaging system first developed by Hounsfield (1973). X-ray CT is a technique to show the spatial distribution of X-ray linear absorption coefficients of samples. The linear absorption coefficient depends on the density and chemical composition of samples and the used X-ray energy. Higher density and higher atomic numbers result in higher attenuation of X-rays. X-ray CT produces images in which grayscale corresponds to the X-ray linear attenuation coefficient. Individual CT images are referred to as slices (see Fig. 3(a)). By stacking of sequential slices, data for a complete volume can be ob-

(a)

(b)

(c)

Fig. 3.   (a) Geometry of the X-ray CT image. (b) Cross sections on (left) *y-z* and (right) *z-x* planes every 15 and 12 units of in-plane resolution (0.313 mm) for Section 307-U 1318A-5H4, 22–72 cm. Core top is on the left-hand side. Grayscale bar shows CT number. Some IRD are shown in white circles on *y* = 72 plane. The black line shows the location of profile in Fig. 3(c). (c) CT number profile along the line on *y* = 72 plane in Fig. 3(b).

lithified sediments may be discriminated by CT numbers. Figure 2 also clearly shows significant differences in CT numbers for pebbles and their surrounding sediments whose CT numbers are around 1380 and 2460 respectively.

2.3 X-ray radiograms

X-ray radiography is based on the differential transmission of radiation through a sample. This technique is non-destructive, and provides density variations within a sample. To obtain a better image, the half-round core sample was cut and divided into slabs with dimensions of $200 \times 30 \times 7$ mm; with z, x, y directions in Fig. 3(a), respectively. Three 7 mm-thick slabs, s1, s2, and s3, along the direction from core top to core bottom, are prepared to accentuate sedimentary structures and to image ice-rafted debris (IRD). s1 and s3 are cut out from the central part of the half-round core sample from 7 mm up to 14 mm in depth intervals, however s2 is cut from the core surface in depth intervals of up to 7 mm, avoiding the pebble. X-ray radiographs of slab samples were taken using a SOFRON STA-10050 X-ray unit at the Geological Survey of Japan, AIST, in November 2005, using a voltage of 40 kVp, a current of 3.5 mA and an exposure time of 40 seconds. X-ray radiographs were directly exposed on FUJIBRO WP FM3 photographic paper. Dark/light color in image indicates low/high density (high/low X-ray transmission), respectively.

2.4 Density measurements

The shipboard GRA bulk density measurements were carried out on the unsplit core with sampling interval and measurement width of 5 cm and ∼5 mm, immediately after the core liner is cut into sections in May 2005 (Ferdelman *et al.*, 2006). This measurement is based on the principle that the ^{137}Cs attenuation, mainly by Compton scattering, of a collimated beam of gamma rays passing through a known volume of sediment is related to material density (Boyce, 1976). The obtained GRA bulk density in this core section ranges from 1.98 to 2.04 g/cm^3.

Density measurements by Pycnometer (MAD density) using discrete core specimens of ∼8 cm^3 (Blum, 1997) were conducted after splitting core in May 2005. The MAD density is 1.877 g/cm^3 at 42.90 mbsf (Ferdelman *et al.*, 2006), which is in good agreement with the GRA density. This value is the direct estimate of the average bulk density, and can be used to calibrate the GRA bulk density data.

Bulk density measurements by the mass-volume method were also carried out at the Geological Survey of Japan, AIST, in June 2008. Discrete samples from the lithified host sediments of about 7 cm^3 were selected using plastic cubes at 5 cm intervals from as close to the center of the core as possible to measure density. Obtained wet-bulk density was determined to be 1.65 to 1.86 g/cm^3. On the other hand, the density of the sedimentary pebble sample at about 60 cm was determined to be 2.74±0.04 g/cm^3 using the water saturation method at the Geological Survey of Japan, AIST, in August 2007 (Furukawa, personal comm.).

3. Results and Discussions

X-ray CT images on *y-z* and *z-x* planes as defined in Fig. 3(a) are shown in Fig. 3(b), although image reconstructions in any directions are possible after the data acquisition. In Fig. 3(b), X-ray CT-generated grayscale images were constructed using histogram equalization with the lower limit value of water, which provides contrastive images for structure observations. Left and right sides of Fig. 3(b) show cross sections on *y-z* and *z-x* planes every 15 and 12 units of in-plane resolution (0.313 mm), respectively. The core is not perfectly aligned to the center of stage of X-ray CT scanner; therefore the core appears tilted in the images. Two holes at 36.1 and 74.0 cm, due to shear strengths measurements with a hand held torvane sampler on board, are clearly visible in both *y-z* and *z-x* planes. Curved laminar structures possibly due to drilling and sampling processes, are observed near the linear. Significant differences in CT numbers among sediments, IRD (some examples are highlighted by white circles on $y = 72$ plane in Fig. 3(b)), and pebble at 60 cm are represented by grayscale. Although CT numbers of sediments are similar (clearly shown in Fig. 2), laminae appear in CT number variations by the enhanced images as shown in Fig. 3(b), implying that these structures retain density contrasts. Figure 3(c) shows the CT number variations along the black line on $y = 72$ plane in Fig. 3(b). CT number difference between peak and trough values are approximately 100–200 as in Fig. 3(c), and it corresponds to 0.1–0.2 g/cm^3 changes in density, large enough to discriminate density contrasts. Using the core sedimentation rate of 7.1 cm/ka (Titschack *et al.*, 2009), CT number variations are assessed with temporal resolution of the order of ten years.

Figure 4 combines (a) X-ray radiograph, (b) X-ray CT image, and (c) line-scan digital core images of the sample with a total length about 50 cm. Note that the "archive-half" was described visually and photographed. X-ray CT and X-ray radiograph was performed using the "working-half". In Fig. 4(b), $y = 72$ plane was chosen, which almost corresponds to about 14 mm depth from the core surface, avoiding data gaps at 36.1 and 74.0 cm.

Three kinds of images as shown in Fig. 4 are compared with each other to highlight their characteristics, advantages, and limitations. Line-scan digital core images provide detailed visual information on the surface. X-ray radiograph system produces 2-D images of internal 3-D structures, but in a single 2-D shadow projection the depth information is completely mixed. X-ray radiographs reveal laminae on a millimeter scale more clearly but nonquantitatively, and highlight many IRDs as bright spots against dark-colored background sediments, partly because they reflect an integration of information over the slab thickness of 7 mm. On the other hand, X-ray CT system allows us to visualise and measure complete 3-D object structures without sample preparation, and X-ray CT image can be sliced in any sections and reveal sedimentary and post sedimentation structures and materials that cannot be seen on the split core surface. However, because of the lower resolution of X-ray CT images, smaller targets may not be imaged.

Variations in grayscale values of the line-scan digital core image, X-ray CT image and X-ray radiograph reflect laminae. Based on the line-scan digital core image, laminae curved downwards due to drilling disturbance close to liners were frequently observed, which are easily recognized by X-ray CT image. The X-ray CT image (Fig. 4(b)) also
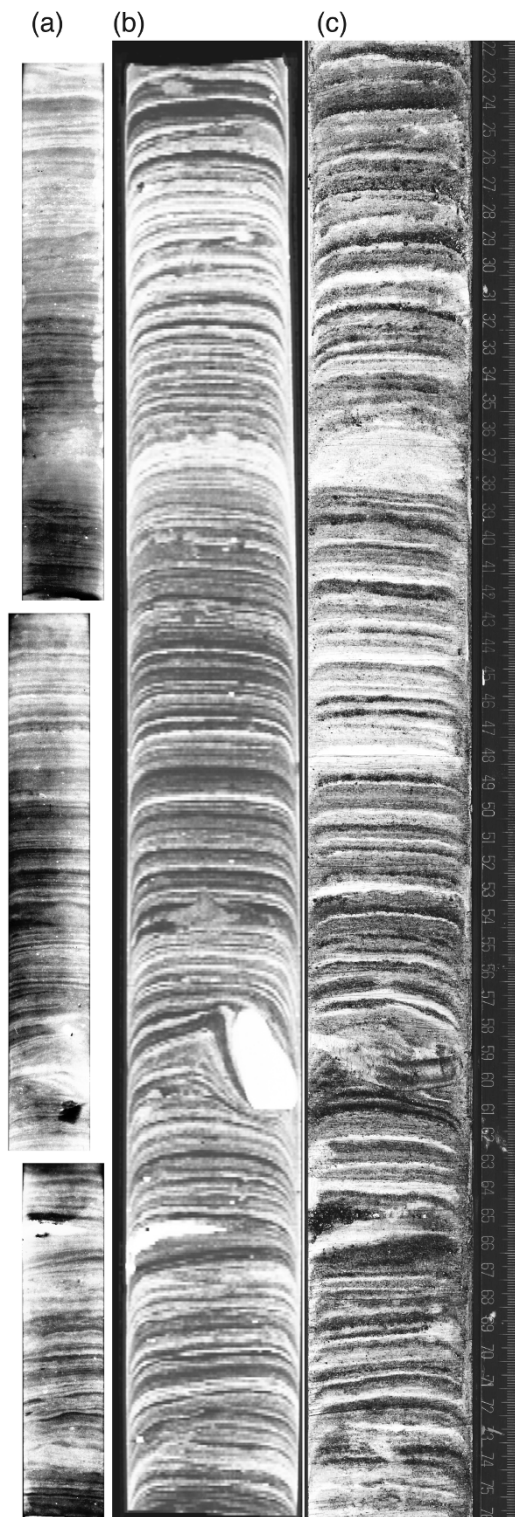
Fig. 4. (a) X-ray radiogram, (b) X-ray CT image on $y = 72$ plane, (c) line-scan digital core image enhanced by histogram equalization, of half-round core sample from Section 307-U1318A-5H4, 22–72 cm. Note that X-ray CT image and X-ray radiogram are mirrored images to correspond to the line-scan digital core image. Scale attached (c) is used for locations mentioned in the text.
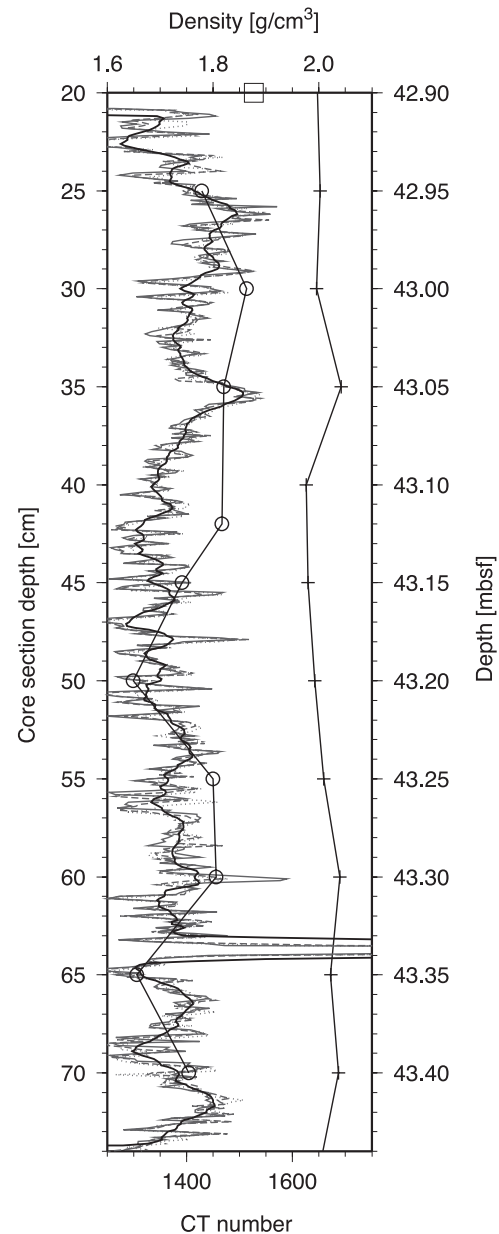

Fig. 5. CT numbers (gray line), GRA gamma densities (crosses), mass/volume-derived densities (circles), and MAD density (square), for Section 307-U 1318A-5H4, 22–72 cm. Gray solid, dashed, and dotted lines represent profiles of CT number at $x = 150$, 160, and 170, respectively. These profiles are obtained using average of 5 profiles from $y = 80$, 90, 100, 110, and 120. The solid line represents a moving average of 10 CT numbers for the core section depth using 15 profiles.

captures disturbance of laminae near the pebble at 60 cm. This pebble is clearly captured in the X-ray CT images but cannot be seen on the split core surface. However, disturbances of original sedimentary structures at corresponding range are evidenced in the line-scan digital core image as shown in Fig. 4(c).

Figure 5 shows variations in CT numbers taken along the core axis, with GRA bulk densities on board and laboratory-measured densities as described in Section 2.4. Densities obtained from GRA measurements and mass/volume methods are not well correlated with each other. This difference may come from the different sample area and volume used for measuring densities: The GRA density measurement provides an estimate integrated over an irradiated cylindrical volume with a diameter of 66 mm and a width of ~5 mm of the whole core sample (Boyce, 1976) and densities were determined by the mass/volume method on discrete cube
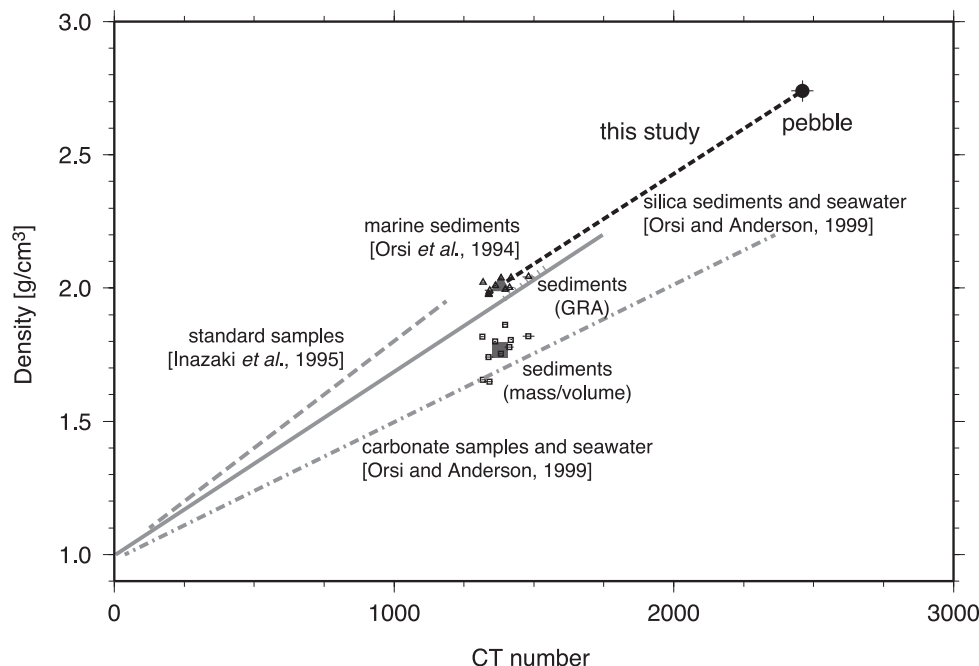
Fig. 6. Scatterplot illustrating the relationship between CT number and wet bulk density. Open triangles and squares show all the data points for densities obtained from the GRA measurement and the mass/volume method, respectively. The accompanying horizontal bars represent CT number distribution in the corresponding area to be used for density measurements. Solid gray triangle and square indicate average densities of host sediments by the GRA measurements and the mass/volume method, respectively. The solid circle indicates the density of a pebble by the water saturation method with the measurement error. The horizontal bar of the solid circle shows the full-width at half maximum (FWHM) of CT number distribution as a proxy for estimating data range. Thick gray dashed and dotted lines were determined by Inazaki *et al.* (1995) and Orsi *et al.* (1994). Thick gray solid and one-dotted lines were determined by least-squares analysis for silica sediments and carbonate samples by Orsi and Anderson (1999). Dashed line was determined in this study.

samples (~ 7 cm^3) that were cut from split core sections. The GRA bulk densities are about 0.24 g/cm^3 higher on average than those of the mass/volume method. One of the plausible reasons is that cores gradually dried after coring, even though the core sample was contained inside plastic liner. The GRA bulk densities show no significant change throughout the 50-cm long core sample, however the densities obtained from mass/volume method show a wider range than those of GRA measurements. It may be related that samplings in the mass/volume method are frequently biased due to uneven distribution of materials and samples do not represent the exact average at the position.

Regions near the center of core excluding the pebble at 60 cm and two data gaps at 36.1 cm and 74.0 cm are chosen to show CT number variations in Fig. 5. CT numbers in each voxel of reconstructed CT image are plotted as a function of core section depth. Each average value at $x = 150$, 160, and 170, using 5 data at $y = 80, 90, 100, 110, 120$ is used to exclude outliers and to reflect a larger spatial area, as shown in gray lines in Fig. 5. Although the direction of core section depth is not exactly parallel to sediment layer stratification, each CT number variations and three average values show similar trends with peaks in phase. As mentioned before, there might be expected a sort of relation between variations of CT number and densities. Gray lines in Fig. 5 show density variations corresponding to distinct sedimentary sequence, which clearly shown in different colours in Fig. 4. Figure 5 also shows a moving average of 10 CT numbers for the core section depth using 15 profiles at $(x, y) = ([150, 160, 170], [80, 90, 100, 110, 120])$,

to capture long-term trends.

Two GRA density peaks at depths of 35 and 60 cm are shown in Fig. 5, although GRA density changes are relatively small all through this sample. The peak at 35 cm is also recognized at the similar depth in the line-scan digital core image and X-ray radiograph as a bright-colored area in Figs. 4(a) and (c), which corresponds to higher CT number. At this cross section depth, density by mass/volume method is rather high. The GRA density has the second highest value at 60 cm through this sample, where averaged CT number also has a peak at this depth. On the other hand, CT number shows a high peak at 64 cm. This part coincides with a concentration of a white fine-sand layer, only 5–10 mm thick in the line-scan digital core image, X-ray CT image and X-ray radiograph as shown in Fig. 4. However, densities obtained from GRA measurements and mass/volume methods do not correspond to this high CT number. The peak at 64 cm may be out of the target area of GRA density measurements collected at 5 cm intervals with the measurement width of ~ 5 mm.

Several attempts have been made to convert CT numbers to equivalent sediment bulk density and have verified the linear correlation between bulk density and X-ray attenuation (e.g., Orsi *et al.*, 1994), although there are many uncontrollable variables, including machine-dependent parameters and statistical parameters of samples such as mean value and standard deviation of CT numbers. Previous calibration experiments on the Technicare Δ-100 CT scanner at 120 kV/25 mA using marine sediments from the northern Gulf of Mexico continental shelf, showed a lin-

ear response between bulk density (ρ) and CT number (HU) described by $\rho = (0.783/1000)\text{HU} + 0.869$ (Orsi *et al.*, 1994). They estimated the average density resolution of the system much smaller than 0.01 g/cm^3 with the bulk density range from 1.96 to 2.08 g/cm^3. A calibration procedure by Orsi and Anderson (1999) using two types of material showed the difference of gradient between the curve for SiO$_2$ and CaCO$_3$ CT number versus bulk density plots, namely $\rho = (0.689/1000)\text{HU} + 0.997$ and $\rho = (0.516/1000)\text{HU} + 0.981$ over a range of 1.0 and 2.2 g/cm^3. Inazaki *et al.* (1995) indicated that the accuracy of bulk density measurements estimated from the CT number is better than ± 0.02 g/cm^3 by calibration with known standards using medical X-ray CT system (TCT-700S) at 120 kV/55–200 mA. Their suggested linear regression is $\rho = \text{HU}/1250 + 1.00$, using water glasses and pressed bentonites with bulk density ranges between 1.10 and 1.95 g/cm^3.

Figure 6 shows a relationship between CT numbers and measured densities by the GRA and the mass/volume method of host sediments. Densities obtained by the mass/volume method show smaller values than those from the GRA measurements. The density of a pebble by the water saturation method was also plotted. Small variations in CT number for the pebble of sedimentary origin may reflect that pebble material is rather homogeneous. Densities by the GRA measurements of host sediments and pebble fall roughly on the same trend using silica sediments by Orsi and Anderson (1999). Based on CT number and density data obtained from the GRA measurements and pebble, CT number has a linear relationship with density: $\rho = (0.677/1000)\text{HU} + 1.0756$, over a range of 2.0 and 2.7 g/cm^3. Although data are not evenly distributed over this density range, a medical X-ray CT system respond a linear relationship in density up to 2.7 g/cm^3. However, this obtained linear relation represents a different offset from that shown by silica sediments (Orsi and Anderson, 1999). Further developments of the relationship between CT number and density are required to conduct more quantitative analysis.

Standard conventional techniques for bulk density analysis in sediment cores use raw data from GRA or mass/volume method. These density values obtained from samples represent the gross average. Neither have a spatial resolution better than X-ray CT data-derived density. Moreover, X-ray CT data-derived density offers advantages over these standard conventional techniques as it gives a three-dimensional distribution anywhere in the sample. Also, because of the simple process of the conversion from CT number to density, it is expected to reduce the possibility of human error.

4. Conclusions

Three-dimensional quantitative analysis using X-ray CT combined with X-ray radiographs and line-scan digital core images of a marine sequence recovered during IODP Expedition 307 in the Porcupine Basin is an effective method for core characterization. This paper confirms that X-ray CT proves to be a relatively quick and accurate method for high-resolution and non-destructive analysis of three-

dimensional internal structures of core samples without the special sample preparation. A medical CT system at relatively low resolution provides an image of the large-scale features and allows correlation with core samples, and has generally been used due to their availability and relative ease of use. CT scanning just after coring and before splitting may be efficient to avoid a degradation of cores. Effective and efficient use of X-ray CT systems allows for the possibility for rapid systematic characterization of three-dimensional structural features, and may improve sub-sampling and core-processing procedures. Because X-ray attenuation is sensitive to density variations, X-ray CT systems also offer the possibility of quantitative density measurement. Its rapid and quantitative results can easily be used to map subtle detailed density variations in three-dimensions.

References

Ashi, J., Computed tomography scan image analysis of sediments, in *Proc. ODP, Sci. Results*, edited by Shipley, T. H., Y. Ogawa, P. Blum, and J. M. Bahr, **156**, 151–159, 1997.

Blum, P., Physical properties handbook: a guide to the shipboard measurement of physical properties of deep-sea cores, *ODP Tech. Note*, **26**, 1997.

Boyce, R. E., Definitions and laboratory techniques of compressional sound velocity parameters and wet water content, bulk density, and porosity parameters by gravimetric and gamma-ray attenuation techniques, in *Initial Reports Deep Sea Drilling Project 33*, edited by Schlanger, S. O., E. Jackson *et al.*, 931–958, US Government Printing Office, Washington, DC, 1976.

Ferdelman, T. G., A. Kano, T. Williams, J.-P. Henriet, and the IODP Expedition 307 Scientists, Modern carbonate mounds: Porcupine Drilling, in *Proceedings of the Integrated Ocean Drilling Program*, Volume 307: College Station, Texas, Integrated Ocean Drilling Program Management International, Inc., doi: 10.2204/iodp.proc.307.2006, 2006.

Hounsfield, G. N., Computerized transverse axial scanning (tomography): Part I. Description of system, *Br. J. Radiol.*, **46**, 1016–1022, 1973.

Inazaki, T., Y. Inouchi, and T. Nakano, Use of medical X-ray CT scanner for nondestructive and quantitative analysis of lake sediments, *Bull. Geol. Surv. Jpn.*, **46**, 629–642, 1995 (in Japanese with English abstract).

Iturrino, G. J., R. A. Ketcham, L. Christiansen, and G. Boitnott, Data report: permeability, resistivity, and X-ray computed tomography measurements in samples from the PACMANUS hydrothermal system, in *Proc. ODP, Sci. Results, 193: College Station, TX (Ocean Drilling Program)*, edited by Barriga, F. J. A. S., R. A. Binns, D. J. Miller, and P. M. Herzig, 1–14, doi:10.2973/odp.proc.sr.193.205.2004, 2004.

Kano, A., T. G. Ferdelman, T. Williams, J.-P. Henriet, T. Ishikawa, N. Kawagoe, C. Takashima, Y. Kakizaki, K. Abe, S. Sakai, E. L. Browning, X. Li, and The IODP Expedition 307 Scientists, Age constraints on the origin and growth history of a deep-water coral mound in NE Atlantic drilled in IODP Expedition 307, *Geology*, **35**, 1051–1054, 2007.

McCullough, E. C., Photon attenuation in computed tomography, *Med. Phys*, **2**, 307–320, 1975.

Mees, F., R. Swennen, M. Van Geet, and P. Jacobs, Applications of X-ray computed tomography in the geosciences, *Geol. Soc., Lond., Special Publications*, **215**, 1–6, 2003.

ODP Information Technology and Data Services, ODP prime scientific data: Collection, archive, and quality, *ODP Tech. Note*, **37**,

doi:10.2973/odp.tn.37.2007, 2007.

Orsi, T. H. and A. L. Anderson, Bulk density calibration for X-ray tomographic analyses of marine sediments, *Geo-Mar. Lett.*, **19**(4), 270–274, 1999.

Orsi, T. H., C. M. Edwards, and A. L. Anderson, X-ray computed tomography: A non-destructive method for quantitative analysis of sediment cores, *J. Sediment. Res.*, **A64**, 690–693, 1994.

Pyrak-Nolte, L. J., C. D. Montemagno, and D. D. Nolte, Volumetric imaging of aperture distributions in connected fracture networks, *Geophys. Res. Lett.*, **24**, 2343–2346, 1997.

Shannon, P. M., P. D. W. Haughton, and D. Corcoran (eds.), The petroleum exploration of Ireland's Offshore Basins, *Geol. Soc., Lond., Special Publications*, **188**, 473 pp, 2001.

Shimazaki, H. and S. Shinomoto, A method for selecting the bin size of a time histogram, *Neural Comput.*, **19**(6), 1503–1527, 2007.

Tanaka, A. and T. Nakano, Data report: three-dimensional observation and quantification of internal structure of sediment core from Challenger Mound area in the Porcupine Seabight off western Ireland using a med-ical X-ray CT, in *Proc. IODP, 307*, edited by Ferdelman, T. G., A. Kano, T. Williams, J.-P. Henriet, and the Expedition 307 Scientists, Washington, DC (Integrated Ocean Drilling Program Management International, Inc.), doi:10.2204/iodp.proc.307.209.2009, 2009.

Titschack, J., M. Thierens, B. Dorschel, C. Schulbert, A. Freiwald, A. Kano, C. Takashima, N. Kawagoe, X. Li, and the IODP Expedition 307 scientific party, Carbonate budget of a cold-water coral mound (Challenger Mound, IODP Exp. 307), *Mar. Geol.*, **259**, 36–46, 2009.

Tivey, M. K. and S. Singh, Nondestructive imaging of fragile sea-floor vent deposit samples, *Geology*, **25**, 931–934, 1997.

Wessel, P. and W. H. F. Smith, New, improved version of the Generic Mapping Tools released, *Eos Trans. AGU*, **79**(47), 579, 1998.

Williams, T., A. Kano, T. G. Ferdelman, J.-P. Henriet *et al.*, Cold-water coral mounds revealed, *Eos Trans. AGU*, **87**(47), 525–526, 2006.

A. Tanaka (e-mail: akiko-tanaka@aist.go.jp), T. Nakano, and K. Ikehara